Applied Surface Science 470 (2019) 129–134

Contents lists available at ScienceDirect

Applied Surface Science

journal homepage: www.elsevier.com/locate/apsusc

Full Length Article

Low-temperature wafer-scale growth of MoS_2-graphene heterostructures

Hyeong-U Kim[a], Mansu Kim[b], Yinhua Jin[a], Yuhwan Hyeon[a], Ki Seok Kim[b], Byeong-Seon An[b], Cheol-Woong Yang[b], Vinit Kanade[a], Ji-Yun Moon[c], Geun Yong Yeom[a,b], Dongmok Whang[a,b], Jae-Hyun Lee[c,*], Taesung Kim[a,d,*]

[a] SKKU Advanced Institute of Nanotechnology (SAINT), Sungkyunkwan University, Suwon 16419, South Korea
[b] School of Advanced Materials Science and Engineering, Sungkyunkwan University, Suwon 16419, South Korea
[c] Department of Energy Systems Research and Department of Materials Science and Engineering, Ajou University, Suwon 16499, South Korea
[d] School of Mechanical Engineering, Sungkyunkwan University, Suwon 16419, South Korea

ARTICLE INFO

Keywords:
MoS_2
Graphene
Heterostructure
Large-scale
PECVD
Hydrogen evolution reaction

ABSTRACT

In this study, we successfully demonstrate the fabrication of a MoS_2-graphene heterostructure (MGH) on a 4 inch wafer at 300 °C by depositing a thin Mo film seed layer on graphene followed by sulfurization using H_2S plasma. By utilizing Raman spectroscopy and high-resolution transmission electron microscopy, we have confirmed that 5–6 MoS_2 layers with a large density of sulfur vacancies are grown uniformly on the entire substrate. The chemical composition of MoS_2 on graphene was evaluated by X-ray photoelectron spectroscopy, which confirmed the atomic ratio of Mo to S to be 1:1.78, which is much lower than the stoichiometric value of 2 from standard MoS_2. To exploit the properties of the nanocrystalline and defective MGH film obtained in our process, we have utilized it as a catalyst for hydrodesulfurization and as an electrocatalyst for the hydrogen evolution reaction. Compared to MoS_2 grown on an amorphous SiO_2 substrate, the MGH has smaller onset potential and Tafel slope, indicating its enhanced catalytic performance. Our practical growth approach can be applied to other two-dimensional crystals, which are potentially used in a wide range of applications such as electronic devices and catalysis.

1. Introduction

Realization of two-dimensional (2D) heterostructures has been intensively studied in view of their unique chemical, physical, and electrical properties [1–4]. Thus far, the main strategy for the preparation of a 2D heterostructure has been based on the sequential stacking of the layered materials using wet or dry transfer methods [5,6]. Ideally, this method allows for a conceptually new class of flexible and transparent films, with applications in batteries, electronic devices, and electrochemical cells [7–9]. However, these methods require time-consuming and complicated transfer processes, which also generate defects or residues at the interface of the 2D heterostructure [10]. The conventional thermal chemical vapor deposition (CVD) method using thermal decomposition of feedstocks, is considered a practical approach for the manufacture of 2D materials, whereby high-quality atomic scale heterostructures over large area can be obtained [11]. In particular, graphene, which is flexible, transparent, and highly conductive, is an ideal template to synthesize various transition metal dichalcogenide (TMDC) materials [12–14]. However, CVD reactions need relatively high growth temperatures (600–1000 °C) [15–17], which is incompatible with the complementary metal-oxidesemiconductor (CMOS) process and can therefore increase the total thermal budget in device fabrication [18–20]. To overcome this limitation, plasma-enhanced CVD (PECVD)-based synthesis technique has been introduced for 2D materials [21,22]. Although initial installation cost of PECVD system is higher than that of typical CVD system, in the presence of accelerated energetic electrons, excited molecules, free radicals, photons, and other active species in the plasma, the controlled growth of 2D materials can be realized at a relatively lower temperature. Our group recently demonstrated the low-temperature growth of uniform MoS_2 on a flexible plastic substrate [23,24].

In view of its tunable band gap and relatively high carrier mobility, MoS_2 has been investigated for applications in future electronic devices [25]. In addition, defects and edges of MoS_2 on the basal plane can act as active catalyst for hydro-desulfurization, due to which MoS_2 is considered as a strong candidate to replace currently used noble Pt catalyst [4,26]. Since Pt, which is considered as the best catalyst for HER, is low in natural abundance and high in cost, alternative catalysts

* Corresponding authors at: SKKU Advanced Institute of Nanotechnology (SAINT), Sungkyunkwan University, Suwon 16419, South Korea (T. Kim).
E-mail addresses: jaehyunlee@ajou.ac.kr (J.-H. Lee), tkim@skku.edu (T. Kim).

https://doi.org/10.1016/j.apsusc.2018.11.126
Received 5 July 2018; Received in revised form 12 November 2018; Accepted 15 November 2018
Available online 15 November 2018
0169-4332/

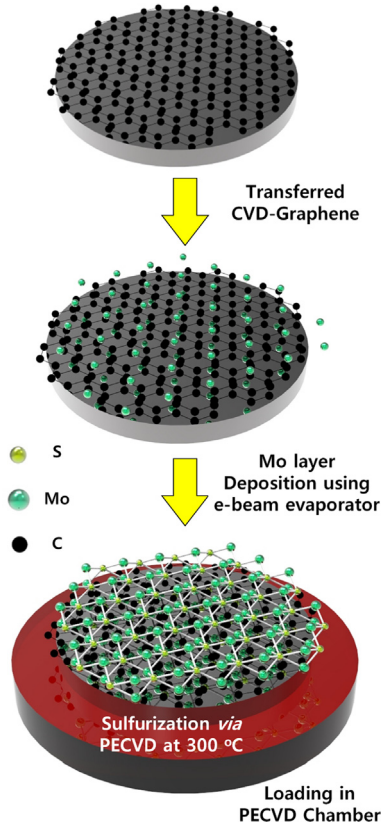

Fig. 1. Schematic illustration of the synthesis of the uniform MGH film via PECVD at 300 °C.

such as metal alloys, TMDs, and composite with TMDs were developed [9,27]. In particular, the combination of MoS_2 with graphene opens up new possibilities in electronic applications and also shows great potential as a catalyst [12,13,28–32]. To the best of our knowledge, however, the direct wafer-scale growth of MoS_2 on graphene at temperatures compatible with CMOS technology has not yet been reported. In this study, we demonstrate the fabrication of a MoS_2-graphene heterostructure (MGH) on a 4 inch wafer at 300 °C. A thin Mo film, which functions as a seed layer, was deposited on transferred graphene using e-beam evaporation after which, sulfurization was carried out using H_2S plasma. Raman spectroscopy and high-resolution transmission electron microscopy (HR-TEM) were used to confirm that MoS_2 layers are uniformly grown on the entire substrate. The chemical composition of MoS_2 on graphene was determined by X-ray photoelectron spectroscopy (XPS); observed XPS data confirmed that the atomic ratio of Mo to S was 1:1.78, which is far beyond the stoichiometric value of the standard MoS_2. To exploit the unique properties of the nanocrystalline MGH film with high density of sulfur vacancy, we tested it as a catalyst for hydrodesulfurization and as an electro-catalyst for the hydrogen evolution reaction (HER) [33].

2. Experimental

2.1. Growth and transfer of monolayer graphene.

Graphene was synthesized on Cu foils (25 μm-thick, Alpha Aesar, 99.99% purity) using a conventional CVD process. Cu foils were placed in a 4 inch diameter quartz tube and after evacuation, H_2 (8 sccm, 99.999%) was introduced into the chamber and the Cu foil was annealed at 1040 °C for 2 h to remove residual impurities. Next, graphene growth was carried out on the Cu foil for 1 h by injecting 30 sccm of CH_4 and 50 sccm of H_2. Finally, the furnace was rapidly cooled to room temperature under H_2 atmosphere. To transfer the CVD-grown graphene layer from the Cu foil, the as-grown graphene sample was coated with a support layer of poly(methyl methacrylate) (PMMA, Microchem) by spin coating. The Cu foil was dissolved in aqueous iron (III) chloride ($FeCl_3$) solution and the PMMA-coated graphene was washed several times with deionized (DI) water before transferring it onto a SiO_2/Si wafer. The PMMA film was then completely dissolved in acetone.

2.2. Direct growth of MoS_2-graphene heterostructure (MGH)

Growth of the MGH structure is schematically illustrated in Fig. 1. A thin film of molybdenum, which serves as a seed layer for the growth of MoS_2, was deposited by e-beam evaporation [21]. The Mo-deposited substrate was loaded into the PECVD chamber for sulfurization. Sulfurization at 300 °C under H_2S and Ar plasma atmosphere for 1.5 h led to the formation of MGH.

2.3. Characterization

The crystallinity and number of layers of graphene and MGH were characterized by Raman spectroscopy (Alpha300 M+, WITec GmbH,

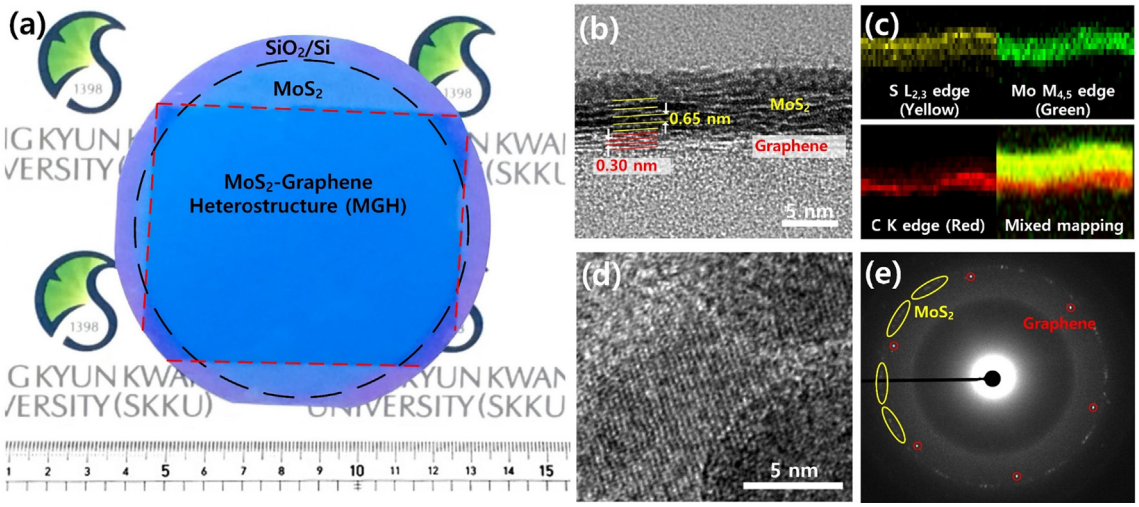

Fig. 2. (a) A photograph of wafer-scale MGH on a 4-inch SiO_2/Si substrate. The rectangular (red dashed) and the circular (black dashed) regions indicate MGH and bare MoS_2 on SiO_2/Si substrate, respectively. (b) Cross-sectional HR-TEM images of MGH (c) Electron energy loss spectroscopy elemental mapping images of MGH, which are derived from the Mo $M_{4,5}$, S $L_{2,3}$, and C K ionization edges. (d) In-plane HR-TEM image of MGH (e) SAED pattern of the MGH shown in Fig. 2(d).

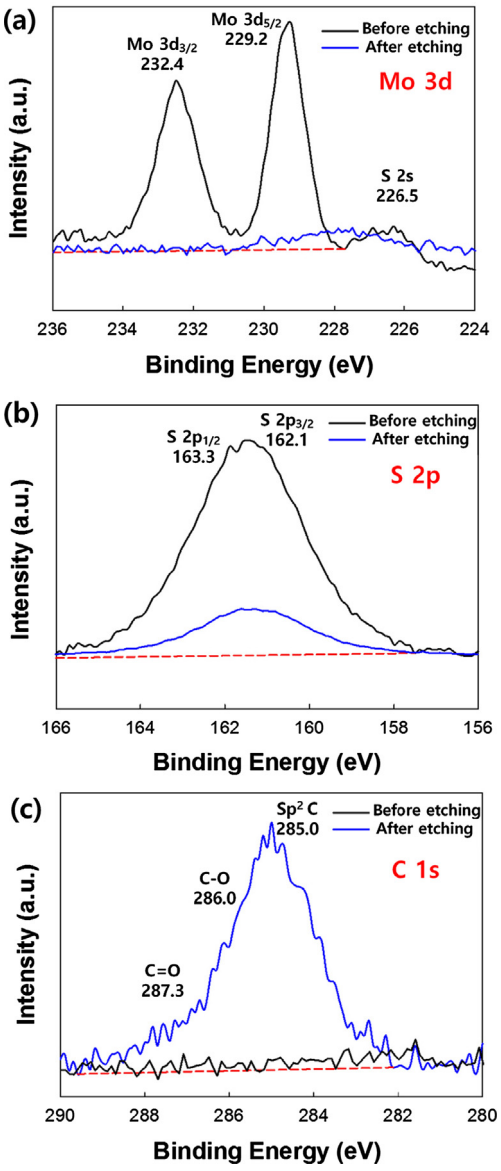

Fig. 3. XPS spectra of an MGH thin film before and after Ar etching for depth profiling (a) Mo 3d (b) S 2p for MoS_2 and (c) C 1s for graphene, respectively.

excitation wavelength of 532 nm and laser power of 2 mW) and HR-TEM (JEM-2100F, JEOL). Samples for cross sectional transmission electron microscopy (TEM) imaging were fabricated using a focused ion beam (FIB, NX2000, HITACHI Ltd.) with a lift-out technique. The TEM samples were etched using Ga^+ ion beam from 30 keV to 5 keV during the FIB milling process. Then a low-energy Ar^+ ion beam of 1 keV was used for final milling to minimize surface damage. The respective chemical compositions of the samples were determined by X-ray photoelectron spectroscopy (XPS, MultiLab 2000, Thermo VG) with Mg Kα X-ray source; during XPS, the take-off angle of the MGH was maintained at 45°. Topological profiles of the thin layers were measured using atomic force microscopy (AFM, NX-100, Park system) and electrochemical data were recorded using an Autolab PGSTAT302N potentiostat (Metrohm Autolab B.V.).

2.4. Electrochemical measurements

All the electrochemical measurements were carried out with a standard three electrode cell using a potentiostat (Autolab PGSTAT302N). A graphite rod (Sigma-Aldrich, 99.995%) and a saturated calomel electrode (saturated KCl) were used as the counter and reference electrodes (SCE, 0.256 V vs. RHE in 0.5 M H_2SO_4), respectively; all the measured potentials were referenced to the reversible hydrogen electrode (RHE) potential. Linear sweep voltammograms (LSV) were traced using a glassy carbon electrode (GCE) (0.196 cm^2, Pine Research Instrumentation, USA) at a scan rate of 2 mV s^{-1} and rotation speed of 1600 rpm. Electrochemical impedance spectroscopy (EIS) was performed in the frequency range 0.01–100,000 Hz at −0.4 V (versus RHE) to determine the series resistance (R_s) and charge-transfer resistance (R_{ct}). All the data presented were corrected with R_s. The GCE was polished with a 0.05 μm Al_2O_3 (Buehler) slurry, rinsed with deionized (DI) water, cleaned in water for 10 s using an ultrasonic cleaner and then washed once again with DI water. The bare glassy carbon electrode was polished to a mirror surface using 0.3 and 0.05 μm Al_2O_3 powders, consecutively, and thoroughly rinsed twice with DI water between each polishing step. Next, the electrode was washed successively in ultra-sonic bath with 1:1 (v/v) HNO_3 aqueous solution, twice in DI water, once in ethanol, and again twice in DI water; finally, the clean electrode was dried in air.

3. Results and discussion

A photograph of the 100-cm^2-area MGH (dark blue rectangular region) shows highly uniform growth of MGH on the 4-inch SiO_2/Si wafer in Fig. 2(a). HR-TEM was conducted to determine both the number of layers and the crystallinity of the MGH. Cross sectional HR-TEM image of MGH and its corresponding electron energy loss spectroscopy elemental mapping images show that top MoS_2 layers of total thickness 6–7 nm are uniformly and continuously grown on the underlying graphene (Fig. 2(b) and (c)). The *d*-spacing of the MoS_2 layers (yellow line) and graphene (red line) is 0.63–0.65 nm and 0.30–0.32 nm, respectively, which is consistent with that measured for typical bulk MoS_2 and graphite (Fig. 2(b)) [15]. An in-plane HR-TEM image of MGH in Fig. 2(d) depicts the overlapping of MoS_2 and graphene layers with grain boundaries. The corresponding selected area electron diffraction (SAED) patterns of the MGH consist of single (red circles) and multiple (yellow circles) sets of diffractions spots with six-fold symmetry originating from the top layer of the nanocrystalline MoS_2 and the bottom graphene layer, respectively, as depicted in Fig. 2(e). We also confirmed that the crystallinity of the bare MoS_2 is similar to that of the MGH in Fig. S1. The overall crystal structure of MGH was elucidated by XRD, where four diffraction peaks at 2θ values of 14.5°, 33°, 39°, and 59°, corresponding to the (0 0 2), (1 0 0), (1 0 3), and (1 1 0) planes, respectively, are seen, as marked in Fig. S2 (JCPDS 37-1492). We note here that the strong (0 0 2) reflection confirms the presence of the layered structure of MoS_2 [34]. The topology of the MGH was investigated by AFM and the root mean square (RMS) value is estimated to be 1.95 nm (Fig. S3).

The chemical states of both the top-MoS_2 film and the bottom-graphene layer in the MGH were analyzed sequentially by depth profiling XPS [35]. The Mo(3d) and S(2p) XPS spectra are presented in Fig. 3(a) and (b). The binding energies of the Mo^{4+} 3d peaks at 229.2 and 232.4 eV corresponding to Mo $3d_{5/2}$ and Mo $3d_{3/2}$, respectively, and the S^{2-} 2p peaks at 162.1 and 163.3 eV, corresponding to the S $2p_{3/2}$ and S $2p_{1/2}$, respectively, confirm the elemental composition of MoS_2 on the surface of the MGH. The atomic ratio of S to Mo is found to be 1.78, which is close to the stoichiometric value of 2 in MoS_2 (Fig. S4) [36]. After measuring the XPS of the MoS_2 layer, plasma etching was carried out by Ar^+ ion beam (4 kW, 6 μA, 3 min). It is seen that after plasma etching, the signals originating from MoS_2 layers disappear but those from the underlying graphene appear. The binding energies of 284.6 eV, 285.2 eV, and 287.1 eV in the C1s core level spectral region, due to sp^2 carbon-carbon, sp^3 carbon-carbon, and carbon-oxygen bonds, respectively, indicate that the carbon atoms maintained the honeycomb structure and are not chemically bonded to Mo and S [37].

To explore the effects of graphene during sulfurization, we have

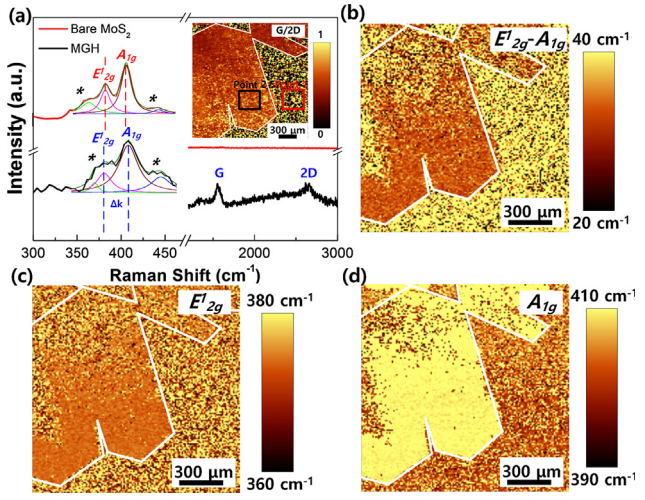

Fig. 4. (a) Representative Raman spectra of MGH and bare MoS_2 at the marked regions (inset shows the Raman mapping of the integrated intensity ratio of the G and 2D). Raman mapping image of MGH for (b) $E^1_{2g} - A_{1g}$, (c) E^1_{2g} and (d) A_{1g} peak, respectively.

simultaneously grown MoS_2 on both graphene and amorphous SiO_2 surfaces; more details on the preparation of partially grown graphene and its transfer on SiO_2/Si substrate are described in Fig. S5. The Raman spectra from both the MGH (black line) and bare MoS_2 (red line) show strong and broad peaks at 373–379 cm^{-1} and 400–406 cm^{-1}, which correspond to the in-plane vibration mode (E^1_{2g}) and out-of-plane vibration mode (A_{1g}), respectively, with weak defect-related satellite Raman peaks (marked as * in Fig. 4 (a)) [38]. In comparison to bare MoS_2, the A_{1g} peak for the MGH is upshifted and the peak separation between E^1_{2g} and A_{1g} (Δk) is increased, indicating that the density of defects increases during sulfurization on the graphene (Fig. 4(b–d)) [13,39]. Interestingly, intensity of peak at 448 cm^{-1}, which correspond to the S vacancy in MoS_2, is significantly increased [38]. Thus, we may infer that the density of point defects (e.g. sulfur vacancies) in MGH should be higher than that in bare MoS_2 [40]. The lattice constant difference of typical metal and MoS_2 is less than 1%, while that of graphene and MoS_2 is about 21.9%. Therefore, growing MoS_2 on the graphene, which has the hexagonal crystal structure and strong interaction, may induce large numbers of point defects compared to growing MoS_2 on the amorphous SiO_2 surface [41–43]. We also note that the S/Mo stoichiometry of MGH from XPS is slightly decrease to 1.78, which indicates a reduction in the total amount of sulfur (Fig. S4). Compared to the Raman spectrum of pristine graphene on SiO_2/Si substrate, the intensities of the G peak (~1580 cm^{-1}), and 2D peak (~2580 cm^{-1}) are not significantly changed after MoS_2 growth, suggesting that the hexagonal carbon structure of graphene is not notably affected by plasma during sulfurization [44].

To exploit the properties of crystalline MoS_2 on conducting graphene, we have investigated the MGH as a catalyst for hydrodesulfurization and as an electro-catalyst in the HER [45]. To demonstrate its catalytic activity, we transferred the MGH film onto a mirror-polished GCE as shown in Fig. S6. Due to the very weak interaction between the graphene layer and the SiO_2 surface, it was possible to delaminate the MGH even in the presence of a MoS_2 film on graphene [2,46]. For comparison, we transferred a bare MoS_2 film on to the pristine GCE using a conventional transfer process. (See Fig. S7)

Electrochemical measurements were performed in 0.5 M H_2SO_4 solution using a typical three-electrode cell setup; the cathodic polarization curves and Tafel plots are shown in Fig. 5. It is seen that 20% Pt/C exhibits a near-zero potential and has the highest HER activity when compared to other catalysts [47,48]. In contrast, the GCE and pristine graphene on GCE electrodes do not show any catalytic behavior.

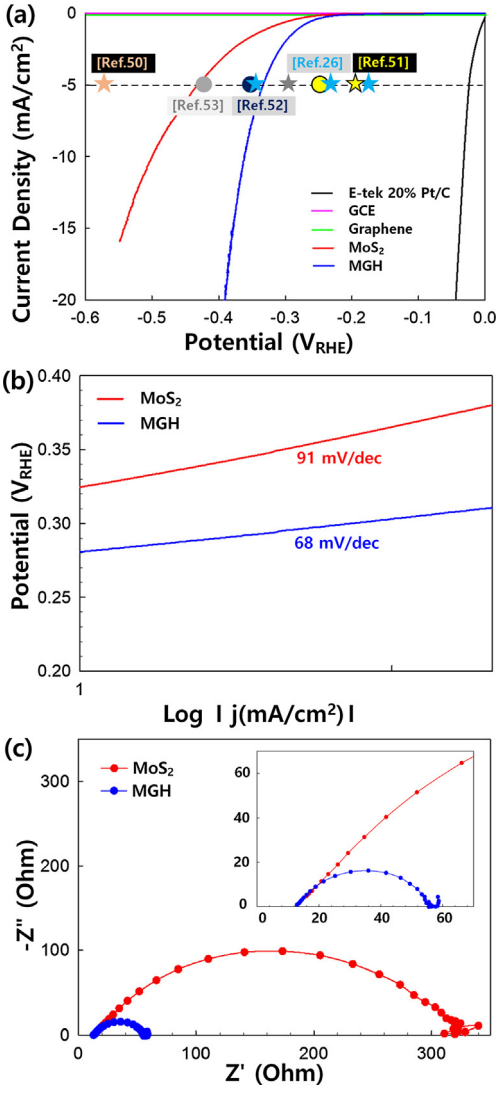

Fig. 5. Electrochemical HER performances of MGH and bare MoS_2 on GEC. (a) Polarization curves measured by LSV along with results from previously published works (b) Tafel plots obtained from polarization curves. (c) EIS of MGH and bare MoS_2 fabricated at 300 °C on GCE; inset shows the spectrum for the specific range from 0 to 70 Ω.

However, the onset over-potential (η) and Tafel slope of the MGH were 0.21 V and 68 mV/dec, which was lower than that of bare MoS_2, pointing to the enhanced catalytic performance of the MGH [49]. It is noted here that MGH shows a better catalytic activity than those previously reported for CVD grown MoS_2 (including exfoliated MoS_2) as shown in Table 1. The onset η values are labeled by stars or circles of different colors in Fig. 5(a) [26,50–53]. The star indicates some sort of treatment such as plasma, annealing, chemical exfoliation, and vacancy for the sample, whereas, those marked by circles indicate that the sample was not subjected to any treatment; the details of the different procedures are given in Table 1. EIS was used to further study the interfacial reactions and electrode kinetics during HER processes for MGH and the bare MoS_2 electrodes. Although the difference in ohmic resistance between the two films is negligible, the charge-transfer resistance of 42 O (Ω) for the MGH film is significantly lower than that of bare MoS_2, which is 311 Ω as shown in Fig. 5(c) [51,54]. Thus, the enhanced catalytic activity of the MGH film electrode can be attributed to be due the following: (1) The large density of grain boundaries and sulfur vacancies on the basal plane in the MGH structure, which give rise to a high density of active sites. (2) The efficient charge transport

Table 1
. A comparison between the various MoS_2-derived HER catalysts in acidic electrolytes.

Catalyst	Synthetic method	Temperature (°C)	η at 5 mA cm^{-2} (V)	Tafel slope (mV dec^{-1})	Refs.
MoS_2	PECVD	300	0.43	91	Present work
MGH			0.33	68	
MoS_2/Au	Mo is evaporated in H_2S atmosphere	550	–	50–60	[45]
O_2 plasma- treated MoS_2	Oxygen plasma treatment after CVD growth	750	0.56	171	[50]
H_2-annealed MoS_2 (500 °C)	Hydrogen annealing after CVD growth		0.56	147	
2H MoS_2	1 T MoS_2 converts to 2H MoS_2	300	0.26	75–85	[51]
1 T MoS_2	Chemical exfoliation	300	0.19	40	
Strained vacancy MoS_2	CVD	750	0.17	60	[26]
Vacancy MoS_2			0.22	82	
Edge-terminated MoS_2			0.36	90	
Edge- terminated MoS_2	CVD	550	0.37	86	[52]
1 T MoS_2	Hydrolysis exfoliation	1000	0.30	98	[53]
2H MoS_2		400	0.45	150	

pathway through the highly conductive graphene layer from the active sites in MoS_2 to the electrode in the MGH film [29,31]. (3) The reduction of band gap at the domain edge of nanocrystalline MGH, which sufficiently decrease hydrogen recombination barrier [55].

4. Conclusion

In conclusion, we have successfully synthesized a 4 inch sized MoS_2-on-graphene heterostructure through a H_2S sulfurization process. The Raman and HR-TEM results reveal that 5–6 MoS_2 layers with a large density of sulfur vacancies and grain boundaries are uniformly grown on the entire substrate. To exploit the nanocrystalline MGH film containing a high sulfur vacancy concentration, we investigated the MGH as a catalyst for hydro-desulfurization and as an electro-catalyst for the HER. When compared to MoS_2 grown from an amorphous SiO_2 substrate, the MGH electrodes have smaller onset potential and Tafel slope, indicating their enhanced catalytic performance. This enhancement can be attributed to the high density of defects (grain boundaries and sulfur vacancies) present in MoS_2 synthesized on graphene, which while increasing the total number of active sites, provide an effective charge transport pathway through the highly conducting graphene layer. We believe that this study will lead to the development of practical strategies for the large-scale synthesis of various 2D heterostructures at low temperatures and thus promote their use in a wide range of applications.

Acknowledgment

This work was supported by the Presidential Postdoctoral Fellowship Program of the Ministry of Education, through the NRF (2014R1A6A3A04058169) and NRF-2017R1A2B3011222. This research was supported by Basic Science Research Program through the National Research Foundation of Korea (NRF) funded by the Ministry of Education (2018R1D1A1B07040292).

Appendix A. Supplementary material

Supplementary data to this article can be found online at https://doi.org/10.1016/j.apsusc.2018.11.126.

References

[1] K. Roy, M. Padmanabhan, S. Goswami, T.P. Sai, G. Ramalingam, S. Raghavan, A. Ghosh, Graphene–MoS_2 hybrid structures for multifunctional photoresponsive memory devices, Nat. Nanotechnol. 8 (2013) 826.
[2] A.K. Geim, Graphene: status and prospects, Science 324 (2009) 1530–1534.
[3] Y.H. Lee, X.Q. Zhang, W. Zhang, M.T. Chang, C.T. Lin, K.D. Chang, Y.C. Yu, J.T.W. Wang, C.S. Chang, L.J. Li, Synthesis of large-area MoS_2 atomic layers with chemical vapor deposition, Adv. Mater. 24 (2012) 2320–2325.
[4] Y. Zhang, Y. Zhang, Q. Ji, J. Ju, H. Yuan, J. Shi, T. Gao, D. Ma, M. Liu, Y. Chen, Controlled growth of high-quality monolayer WS_2 layers on sapphire and imaging its grain boundary, ACS Nano 7 (2013) 8963–8971.
[5] A. Gurarslan, Y. Yu, L. Su, Y. Yu, F. Suarez, S. Yao, Y. Zhu, M. Ozturk, Y. Zhang, L. Cao, Surface-energy-assisted perfect transfer of centimeter-scale monolayer and few-layer MoS_2 films onto arbitrary substrates, ACS Nano 8 (2014) 11522–11528.
[6] H. Van Ngoc, Y. Qian, S.K. Han, D.J. Kang, PMMA-etching-free transfer of wafer-scale chemical vapor deposition two-dimensional atomic crystal by a water soluble polyvinyl alcohol polymer method, Sci. Rep. 6 (2016) 33096.
[7] Y. Fang, Y. Lv, F. Gong, A.A. Elzatahry, G. Zheng, D. Zhao, Synthesis of 2D-mesoporous-carbon/MoS_2 heterostructures with well-defined interfaces for high-performance lithium-ion batteries, Adv. Mater. 28 (2016) 9385–9390.
[8] L. Ma, X. Zhou, L. Xu, X. Xu, L. Zhang, W. Chen, Chitosan-assisted fabrication of ultrathin MoS_2/graphene heterostructures for Li-ion battery with excellent electrochemical performance, Electrochim. Acta 167 (2015) 39–47.
[9] J. Liang, J. Li, H. Zhu, Y. Han, Y. Wang, C. Wang, Z. Jin, G. Zhang, J. Liu, One-step fabrication of large-area ultrathin MoS_2 nanofilms with high catalytic activity for photovoltaic devices, Nanoscale 8 (2016) 16017–16025.
[10] M.F. Khan, M.A. Shehzad, M.Z. Iqbal, M.W. Iqbal, G. Nazir, Y. Seo, J. Eom, A facile route to a high-quality graphene/MoS_2 vertical field-effect transistor with gate-modulated photocurrent response, J. Mater. Chem. C 5 (2017) 2337–2343.
[11] Y. Lee, J. Lee, H. Bark, I.-K. Oh, G.H. Ryu, Z. Lee, H. Kim, J.H. Cho, J.-H. Ahn, C. Lee, Synthesis of wafer-scale uniform molybdenum disulfide films with control over the layer number using a gas phase sulfur precursor, Nanoscale 6 (2014) 2821–2826.
[12] Y. Shi, W. Zhou, A.-Y. Lu, W. Fang, Y.-H. Lee, A.L. Hsu, S.M. Kim, K.K. Kim, H.Y. Yang, L.-J. Li, van der Waals epitaxy of MoS_2 layers using graphene as growth templates, Nano Lett. 12 (2012) 2784–2791.
[13] J.A. Miwa, M. Dendzik, S.S. Grønborg, M. Bianchi, J.V. Lauritsen, P. Hofmann, S. Ulstrup, van der Waals epitaxy of two-dimensional MoS_2–graphene heterostructures in ultrahigh vacuum, ACS Nano 9 (2015) 6502–6510.
[14] H. Ago, H. Endo, P. Solís-Fernández, R. Takizawa, Y. Ohta, Y. Fujita, K. Yamamoto, M. Tsuji, Controlled van der Waals epitaxy of monolayer MoS_2 triangular domains on graphene, ACS Appl. Mater. Interface 7 (2015) 5265–5273.
[15] J. Jeon, S.K. Jang, S.M. Jeon, G. Yoo, Y.H. Jang, J.-H. Park, S. Lee, Layer-controlled CVD growth of large-area two-dimensional MoS_2 films, Nanoscale 7 (2015) 1688–1695.
[16] Y. Zhan, Z. Liu, S. Najmaei, P.M. Ajayan, J. Lou, Large-area vapor-phase growth and characterization of MoS_2 atomic layers on a SiO_2 substrate, Small 8 (2012) 966–971.
[17] X. Wang, H. Feng, Y. Wu, L. Jiao, Controlled synthesis of highly crystalline MoS_2 flakes by chemical vapor deposition, JACS 135 (2013) 5304–5307.
[18] J. Mun, Y. Kim, I.-S. Kang, S.K. Lim, S.J. Lee, J.W. Kim, H.M. Park, T. Kim, S.-W. Kang, Low-temperature growth of layered molybdenum disulphide with controlled clusters, Sci. Rep. 6 (2016) 21854.
[19] H. Takeuchi, A. Wung, X. Sun, R.T. Howe, T.-J. King, Thermal budget limits of quarter-micrometer foundry CMOS for post-processing MEMS devices, IEEE Trans. Elect. Dev. 52 (2005) 2081–2086.
[20] V.T. Renard, M. Jublot, P. Gergaud, P. Cherns, D. Rouchon, A. Chabli, V. Jousseaume, Catalyst preparation for CMOS-compatible silicon nanowire synthesis, Nat. Nanotechnol. 4 (2009) 654.
[21] C. Ahn, J. Lee, H.U. Kim, H. Bark, M. Jeon, G.H. Ryu, Z. Lee, G.Y. Yeom, K. Kim, J. Jung, Low-temperature synthesis of large-scale molybdenum disulfide thin films directly on a plastic substrate using plasma-enhanced chemical vapor deposition, Adv. Mater. 27 (2015) 5223–5229.
[22] S. Kataria, S. Wagner, J. Ruhkopf, A. Gahoi, H. Pandey, R. Bornemann, S. Vaziri, A.D. Smith, M. Ostling, M.C. Lemme, Chemical vapor deposited graphene: From synthesis to applications, Phys. Status Solidi A 211 (2014) 2439–2449.
[23] H. Kim, C. Ahn, G. Arabale, C. Lee, T. Kim, Synthesis of MoS_2 atomic layer using PECVD, ECS Trans. 58 (2013) 47–50.

[24] H.-U. Kim, H. Kim, C. Ahn, A. Kulkarni, M. Jeon, G.Y. Yeom, M.-H. Lee, T. Kim, In situ synthesis of MoS_2 on a polymer based gold electrode platform and its application in electrochemical biosensing, RSC Adv. 5 (2015) 10134–10138.
[25] S. Kim, A. Konar, W. Hwang, J. Lee, J. Lee, J. Yang, C. Jung, H. Kim, J. Yoo, J.Y. Choi, Y.W. Jin, S.Y. Lee, D. Jena, W. Choi, K. Kim, Nat. Commun 3 (2012) 1011.
[26] H. Li, C. Tsai, A.L. Koh, L. Cai, A.W. Contryman, A.H. Fragapane, J. Zhao, H.S. Han, H.C. Manoharan, F. Abild-Pedersen, Activating and optimizing MoS_2 basal planes for hydrogen evolution through the formation of strained sulphur vacancies, Nat. Mater. 15 (2016) 48.
[27] J. Liang, C. Wang, P. Zhao, Y. Wang, L. Ma, G. Zhu, Y. Hu, Z. Lu, Z. Xu, Y. Ma, Interface engineering of anchored ultrathin TiO_2/MoS_2 heterolayers for highly-efficient electrochemical hydrogen production, ACS Appl. Mater. Interface 10 (2018) 6084–6089.
[28] X. Xu, Y. Sun, W. Qiao, X. Zhang, X. Chen, X. Song, L. Wu, W. Zhong, Y. Du, 3D MoS_2-graphene hybrid aerogels as catalyst for enhanced efficient hydrogen evolution, Appl. Surf. Sci. 396 (2017) 1520–1527.
[29] M. Wen, T. Xiong, Z. Zang, W. Wei, X. Tang, F. Dong, Synthesis of MoS_2/gC_3N_4 nanocomposites with enhanced visible-light photocatalytic activity for the removal of nitric oxide (NO), Opt. Exp. 24 (2016) 10205–10212.
[30] J. Liang, G. Zhu, C. Wang, Y. Wang, H. Zhu, Y. Hu, H. Lv, R. Chen, L. Ma, T. Chen, MoS_2-based all-purpose fibrous electrode and self-powering energy fiber for efficient energy harvesting and storage, Adv. Energy Mater. 7 (2017) 1601208.
[31] Y. Li, H. Wang, L. Xie, Y. Liang, G. Hong, H. Dai, MoS_2 nanoparticles grown on graphene: an advanced catalyst for the hydrogen evolution reaction, JACS 133 (2011) 7296–7299.
[32] L. Ma, Y. Hu, G. Zhu, R. Chen, T. Chen, H. Lu, Y. Wang, J. Liang, H. Liu, C. Yan, In situ thermal synthesis of inlaid ultrathin MoS_2/graphene nanosheets as electrocatalysts for the hydrogen evolution reaction, Chem. Mater. 28 (2016) 5733–5742.
[33] B. Hinnemann, P.G. Moses, J. Bonde, K.P. Jørgensen, J.H. Nielsen, S. Horch, I. Chorkendorff, J.K. Nørskov, Biomimetic hydrogen evolution: MoS_2 nanoparticles as catalyst for hydrogen evolution, JACS 127 (2005) 5308–5309.
[34] D.H. Youn, J.-W. Jang, J.Y. Kim, J.S. Jang, S.H. Choi, J.S. Lee, Fabrication of graphene-based electrode in less than a minute through hybrid microwave annealing, Sci. Rep. 4 (2014) 5492.
[35] J.B. Gilbert, M.F. Rubner, R.E. Cohen, Depth-profiling X-ray photoelectron spectroscopy (XPS) analysis of interlayer diffusion in polyelectrolyte multilayers, Proc. Natl. Acad. Sci. 110 (2013) 6651–6656.
[36] P. Beccat, P. Da Silva, Y. Huiban, S. Kasztelan, Quantitative surface analysis by XPS (X-ray photoelectron spectroscopy): application to hydrotreating catalysts, Oil Gas Sci. Technol. 54 (1999) 487–496.
[37] K. Emtsev, F. Speck, T. Seyller, L. Ley, J.D. Riley, Interaction, growth, and ordering of epitaxial graphene on SiC 0001 surfaces: a comparative photoelectron spectroscopy study, Phys. Rev. B 77 (2008) 155303.
[38] S. Bae, N. Sugiyama, T. Matsuo, H. Raebiger, K.-I. Shudo, K. Ohno, Defect-induced vibration modes of Ar + -irradiated MoS_2, Phys. Rev. Appl 7 (2017) 024001.
[39] W.M. Parkin, A. Balan, L. Liang, P.M. Das, M. Lamparski, C.H. Naylor, J.A. Rodríguez-Manzo, A.C. Johnson, V. Meunier, M. Drndić, Raman shifts in electron-irradiated monolayer MoS_2, ACS Nano 10 (2016) 4134–4142.
[40] Y. Ma, Y. Dai, M. Guo, C. Niu, B. Huang, Graphene adhesion on MoS_2 monolayer: an ab initio study, Nanoscale 3 (2011) 3883–3887.
[41] M. Farmanbar, G. Brocks, First-principles study of van der Waals interactions and lattice mismatch at MoS_2/metal interfaces, Phys. Rev. B 93 (2016) 085304.
[42] M. Liu, J. Shi, Y. Li, X. Zhou, D. Ma, Y. Qi, Y. Zhang, Z. Liu, Temperature-triggered sulfur vacancy evolution in monolayer MoS_2/graphene heterostructures, Small 13 (2017) 1602967.
[43] J. Shi, M. Liu, J. Wen, X. Ren, X. Zhou, Q. Ji, D. Ma, Y. Zhang, C. Jin, H. Chen, All chemical vapor deposition synthesis and intrinsic bandgap observation of MoS_2/graphene heterostructures, Adv. Mater. 27 (2015) 7086–7092.
[44] A.C. Ferrari, J. Meyer, V. Scardaci, C. Casiraghi, M. Lazzeri, F. Mauri, S. Piscanec, D. Jiang, K. Novoselov, S. Roth, Raman spectrum of graphene and graphene layers, Phys. Rev. Lett. 97 (2006) 187401.
[45] T.F. Jaramillo, K.P. Jørgensen, J. Bonde, J.H. Nielsen, S. Horch, I. Chorkendorff, Identification of active edge sites for electrochemical H_2 evolution from MoS_2 nanocatalysts, Sci 317 (2007) 100–102.
[46] J.-H. Lee, E.K. Lee, W.-J. Joo, Y. Jang, B.-S. Kim, J.Y. Lim, S.-H. Choi, S.J. Ahn, J.R. Ahn, M.-H. Park, Wafer-scale growth of single-crystal monolayer graphene on reusable hydrogen-terminated germanium, Science 344 (2014) 286–289.
[47] J. Greeley, T.F. Jaramillo, J. Bonde, I. Chorkendorff, J.K. Nørskov, Computational high-throughput screening of electrocatalytic materials for hydrogen evolution, Nat. Mater. 5 (2006) 909.
[48] J. Greeley, I. Stephens, A. Bondarenko, T.P. Johansson, H.A. Hansen, T. Jaramillo, J. Rossmeisl, I. Chorkendorff, J.K. Nørskov, Alloys of platinum and early transition metals as oxygen reduction electrocatalysts, Nat. Chem. 1 (2009) 552.
[49] W. Fu, F.-H. Du, J. Su, X.-H. Li, X. Wei, T.-N. Ye, K.-X. Wang, J.-S. Chen, In situ catalytic growth of large-area multilayered graphene/MoS_2 heterostructures, Sci. Rep. 4 (2014) 4673.
[50] G. Ye, Y. Gong, J. Lin, B. Li, Y. He, S.T. Pantelides, W. Zhou, R. Vajtai, P.M. Ajayan, Defects engineered monolayer MoS_2 for improved hydrogen evolution reaction, Nano Lett. 16 (2016) 1097–1103.
[51] D. Voiry, M. Salehi, R. Silva, T. Fujita, M. Chen, T. Asefa, V.B. Shenoy, G. Eda, M. Chhowalla, Conducting MoS_2 nanosheets as catalysts for hydrogen evolution reaction, Nano Lett. 13 (2013) 6222–6227.
[52] D. Kong, H. Wang, J.J. Cha, M. Pasta, K.J. Koski, J. Yao, Y. Cui, Synthesis of MoS_2 and $MoSe_2$ films with vertically aligned layers, Nano Lett. 13 (2013) 1341–1347.
[53] K. Chang, X. Hai, H. Pang, H. Zhang, L. Shi, G. Liu, H. Liu, G. Zhao, M. Li, J. Ye, Targeted synthesis of 2H-and 1T-phase MoS_2 monolayers for catalytic hydrogen evolution, Adv. Mater. 28 (2016) 10033–10041.
[54] C. Shih, C.-J. Shih, Q.H. Wang, Y. Son, Z. Jin, D. Blankschtein, M.S. Strano, ACS Nano 8 (2014) 5790.
[55] J. Shi, X. Zhou, G.F. Han, M. Liu, D. Ma, J. Sun, C. Li, Q. Ji, Y. Zhang, X. Song, Narrow-gap quantum wires arising from the edges of monolayer MoS_2 synthesized on graphene, Adv. Mater. Interface 3 (2016) 1600332.